Trans Indian Inst Met (2019) 72(6):1537–1540
https://doi.org/10.1007/s12666-019-01621-3

TECHNICAL PAPER

Effect of Tool Rotation Speed on Microstructure and Hardness of Friction-Stir-Welded 9Cr-1Mo Steel

D. Sunilkumar[1] · S. Muthukumaran[1] · M. Vasudevan[2] · S. Paneer Selvi[2] · Madhusudan G. Reddy[3]

Received: 3 September 2018 / Accepted: 14 February 2019 / Published online: 2 March 2019

Abstract In this study, friction stir welding (FSW) of 9Cr-1Mo steel was carried out with tungsten lanthanum oxide (W-La_2O_3) tool to study the influence of tool rotation speeds (200 rpm and 500 rpm) on microstructure and hardness. A smooth defect-free weld joint with complete penetration was accomplished by both rotational speeds. In stir zone (SZ), a fine and lath martensitic microstructure was explored for the 200 rpm and the 500 rpm welds, respectively. The tangible increment in the average hardness of both SZ and thermomechanical affected zone (TMAZ) compared to the base metal (stir zone/TMAZ: $\sim$ 420 VHN, base metal: $\sim$ 212 VHN) was observed due to the effect of phase transformation.

Keywords Friction stir welding · P9 steel · Microstructure · Martensite · Hardness

1 Introduction

The plain 9Cr-1Mo steel indicated as P9 steel has emerged as a structural material for high-temperature applications in the temperature range of 773–823 K, due to its good mechanical properties, high creep strength, and resistance to oxidation as well as corrosion at elevated temperatures [1, 2]. There are certain issues associated with fusion welding of P9 steels such as soft zone formation in fine-grain heat-affected zone (FGHAZ) during post-weld heat treatment (PWHT) [3–5], susceptibility of hydrogen-assisted cracking (HAC) during welding [4], and formation of δ-ferrite in the fusion zone [4, 6]. Therefore, by controlling weld peak temperature lower than the lower critical transformation temperature (Ac_1) of the material, PWHT can be avoided. Such precise control can be executed by FSW where weld temperature and microstructural variation can be controlled [7]. As FSW is a solid-state welding process, the defects associated with melting and solidification will be absent. As rapid tool wear is challenging issues during FSW of high-strength and high-temperature material, high-temperature wear strength is an essential requirement for tool material. For this application, polycrystalline cubic boron nitride (PCBN), highly refractive materials, and tungsten (W)-based alloys are most commonly used as a tool material. FSW of high-strength and high-temperature material produces intact joints with good tool durability by PCBN and highly refractive materials [8]. However, material cost is a limiting factor for selecting this tool material. Hence, in this present study, W-La_2O_3 tool has opted for welding of 9Cr-1Mo steel. The tungsten-based tool shows moderately high strength, toughness, and hardness at elevated temperature. The occurrence of lanthanum oxide in the tungsten matrix impedes dislocation motion of tungsten grains at higher temperature [8, 9]. Thereby, it furnishes the superior strength and toughness. In FSW, the parameter such as tool rotational speed, weld traverse speed, forge pressure, tool geometry, and its tool material selection are the imperative parameters which decide the strength of the weld joint. Out of this, tool

✉ D. Sunilkumar
sunichink@gmail.com

[1] Department of Metallurgical and Materials Engineering, National Institute of Technology, Tiruchirappalli 620015, India

[2] Materials Development and Technology Division, Indira Gandhi Centre for Atomic Research, Kalpakkam 603102, India

[3] Material Joining Group, Defence Metallurgical Research Laboratory, Hyderabad 500058, India

rotational speed is the key parameter that determines the peak temperature and the cooling rate experienced during FSW. Therefore, in the present study, the effect of tool rotational speeds on the microstructure and hardness of the joint has been investigated.

2 Materials and Methods

The P9 steel plates of dimensions 300 mm × 250 mm × 3 mm were used in the present study, and its chemical composition is presented in Table 1. FSW joint configuration and cylindrical tool geometry used in the present study are shown in Fig. 1a. FSW process parameters and the corresponding heat input are presented in Table 2. The heat input (H.I) was calculated based on the equation specified below [10]. The specimens were taken from the radiographically qualified welded joint, metallographically prepared followed by electropolishing for microstructure characterization by electron back-scattered diffraction (EBSD) (FEI quanta 200 HV SEM with EDX OIM). The elemental composition of the weld zone was studied by energy-dispersive spectroscopy (EDS) (Inca Penta FETX3-modal 7537) which was equipped with SEM (Cam Scan 3200). The hardness measurements were carried out across the weld by Vicker's microhardness tester.

$$H.I = \frac{\boldsymbol{\varepsilon 2\pi rT}}{\boldsymbol{1000\vartheta}} \quad (1)$$

where **ε**—dimensionless factor indicating process efficiency, **r**—tool rotational speed rev min^{-1} **T**—average steady-state spindle torque (Nm), ϑ—traverse speed (mm min^{-1}).

Table 1 Chemical composition of P9 steel plate

Element	C	Mn	P	S	Si	Ni	Cr	Mo	Fe
wt (%)	0.12	0.502	0.020	0.0008	0.50	0.20	8.80	0.95	Bal.

Table 2 FSW parameters employed during FSW of P9 steel plate

Tool rotational speed (rpm)	Traverse speed (mm min^{-1})	Tilt angle (°)	Average torque(Nm)	Heat input (KJ mm^{-1})
200	30	2.5	170	3.92
500	30	2.5	90	5.18

3 Results and Discussion

In this present study, JMatPro software was used for predicting Ac_1 and upper critical (Ac_3) transformation temperature for the given P9 base metal. It was found that the ferrite-to-austenite phase transformation started at Ac_1 which was 1079 K (806 °C) and finished at Ac_3 accounting to 1169 K (896 °C). The peak temperature experienced in the SZ during FSW was calculated based on the theoretical formula explained in the previous studies [11].

$$T = K\left(\frac{\omega^2}{\vartheta \times 10^4}\right)^{\propto} T_m \quad (2)$$

where ω is tool rotational speed (rpm), ϑ is welding traverse speed (mm min^{-1}), T_m is the melting point of material, and K, α are constants (K = 0.64, α = 0.04) [11]. The peak temperatures calculated from the above relations were approximately 1053 K and 1133 K for the tool rotational speed of 200 rpm and 500 rpm, respectively. It was noticed that the maximum peak temperature experienced at the tool rotational speed of 200 rpm was well below the lower critical transformation temperature (Ac_1). And, the tool rotational speed of 500 rpm peak temperature was between Ac_1 and Ac_3. The low-magnification optical microscopic view of friction-stir-welded P9 steel plate with two different rotational speeds viz., 200 rpm and 500 rpm, is shown in Fig. 1b. Transverse macrograph profile showed that defect-free joints were achieved with full penetration. It showed that the welding heat input used in the present

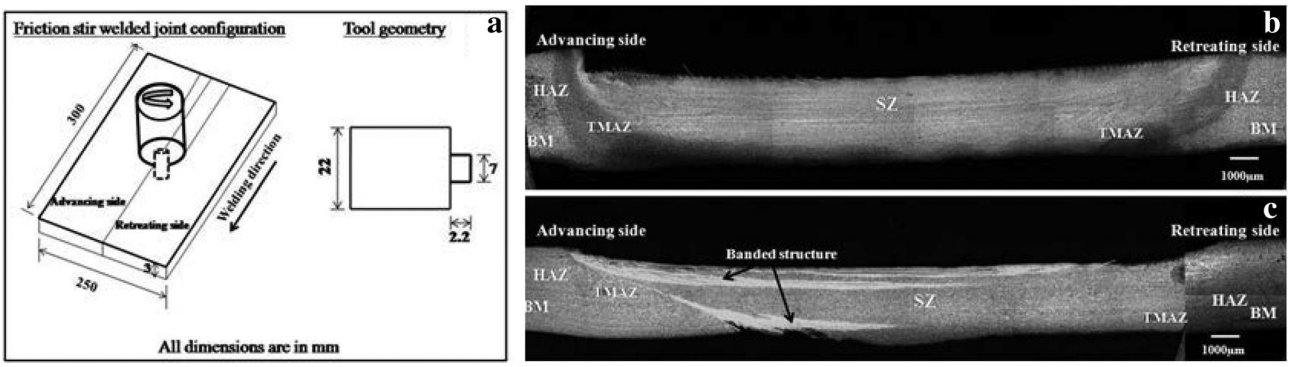

Fig. 1 **a** FSW joint configuration and tool geometry. **b** Optical low-magnification view of friction-stir-welded P9 steel specimen with 200 rpm and **c** 500 rpm

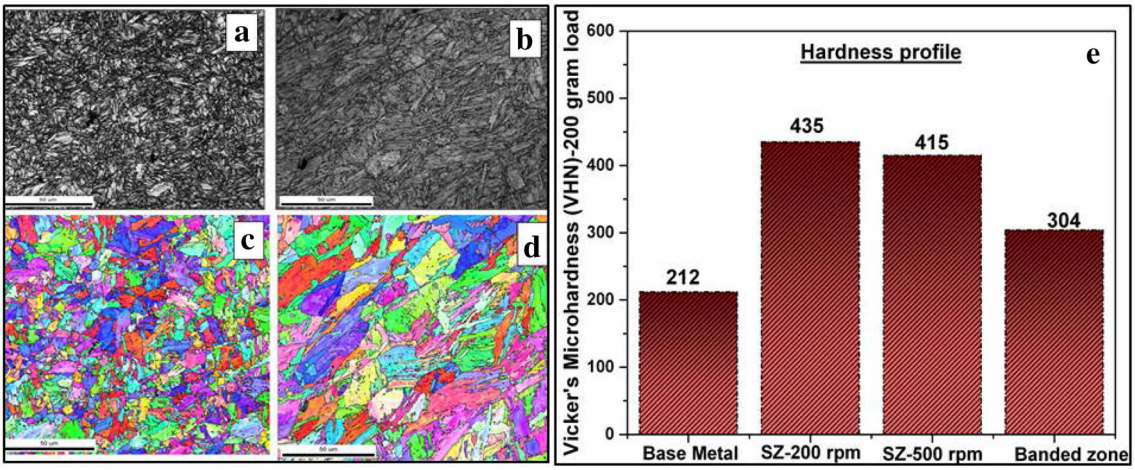

Fig. 2 Grain boundary orientation maps **(a) (c)** 200 rpm; **(b) (d)** 500 rpm; **(e)** hardness measurement of the weld joint

study was sufficient to weld 3-mm-thick P9 steel plates. The cross-sectional view of weld highlighted that the shape of the weld was similar to a basin shape. It explained that the metal flow during FSW was dominated by tool shoulder [12]. Also, the micrograph clearly showed that the weld with the rotational speed of 500 rpm had undergone more deformation than the weld with 200 rpm. Additional features such as a banded structures were found in the advancing side of 500 rpm weld. Microscopic view of this banded structure was explained in a subsequent section. Comparative evaluation between tool rotational speeds of 200 rpm and 500 rpm showed that an increase in tool rotational speed increased the heat input as well as plastic deformation resulting in a wider weld nugget. Using cursor position in the optical microscopy, the combined layer width of TMAZ and HAZ was measured and observed to be 1.35 mm for 200 rpm and 2.63 mm for 500 rpm, respectively.

The SZ microstructure and corresponding hardness profile are shown in Fig. 2. EBSD grain orientation map revealed that there was no preferred grain orientation in the stir zone matrix of both 200 and 500 rpm weld (refer Fig. 2). Even though the peak temperature experienced during friction stir welding was slightly below the Ac_1 temperature for 200 rpm weld, fine martensite was observed due to the extensive plastic deformation during FSW and higher hardenability of P9 steel. However, in the case of 500 rpm weld, the stir zone showed the typical lath martensitic structure. This microstructure portrayed that the peak temperature experienced during 500 rpm weld went above the Ac_1 temperature of the base material. The SZ microstructure features proved that the peak temperature calculated based on the empirical relation was in good agreement with microstructure evolution.

During FSW, the deformed zone by stirring action experienced dynamic recovery and recrystallization. The grain size comparison between stir zone matrix of 200 rpm and 500 rpm weld revealed that finer grain size existed for the 200 rpm weld ($\sim$ 4 μm) than that at 500 rpm weld ($\sim$ 5.9 μm). The base metal grain size was approximately 12 μm. Therefore, a significant grain refinement took place through dynamic recrystallization during FSW. The SEM microscopic view of the banded zone was found in the advancing side of 500 rpm weld and is shown in Fig. 3. Using SEM equipped with EDS, a point analysis was carried out, and the presence of tungsten was discovered in the banded zone. It was due to the tool wear caused by higher frictional load associated with higher rotational

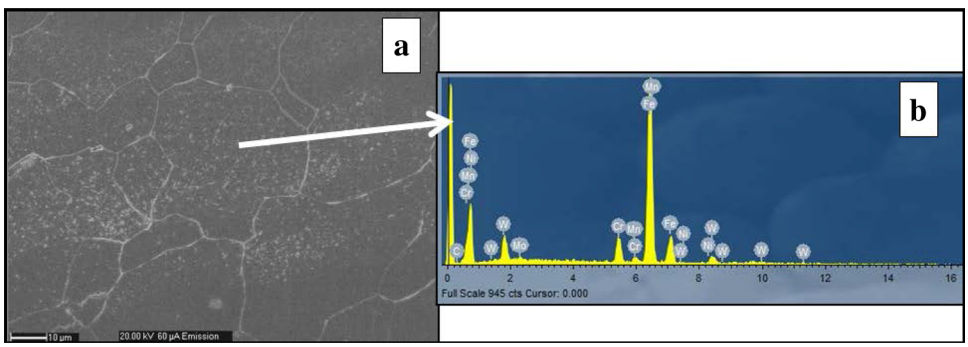

Fig. 3 **a** SEM view of banded structure. **b** Corresponding EDS point analysis spectrum

speed, and it promoted soft ferrite grains in the stir zone matrix. Therefore, in the hardness profile of the weld at 500 rpm, there was a drop in the hardness wherever the banded structure was evolved. However, there was no much significant variation in the hardness of 200 rpm weld from stir face to stir root which confirmed the homogeneity in the microstructure. The hardness of the base metal, SZ, and banded zone found in the SZ matrix of 500 rpm is shown in Fig. 2e. Maximum hardness in the stir zone for both 200 rpm and 500 rpm weld was attributed to the strengthening effect of martensite with high dislocation density. Also, SZ hardness for 200 rpm showed comparatively higher (about 20 VHN) value than 500 rpm due to the finer grain structure. Microstructure and hardness measurement showed that PWHT was mandatory to temper the martensitic microstructure and improved the ductility. The detailed investigations of PWHT followed by microstructure characterization and mechanical properties evaluation are under progress.

4 Conclusion

1. Microstructure characterization evidently showed that stir zone consists of deformed fine martensite in the 200 rpm weld and lath martensitic structure in the 500 rpm weld.
2. FSW employed with low rotational speed can limit the width of TMAZ and HAZ.
3. FSW carried out at low rotational speeds (< 200 rpm) develops peak temperatures in the SZ which is well below the transformation temperature of the base metal. There is no formation of martensite in the weld metal. Hence, PWHT can be avoided.
4. This study proves that P9 steel plate can be welded with the help of W-La_2O_3 tool. There is the absence of tool wear in the lower rotational speed weld, which signifies the better operating life of the tool.

References

1. Nagaraju S, Vasantharaja P, Brahadees G, Vasudevan M, and Mahadevan S, *J Mater Eng Perform* **26** (2017) 5938.
2. Arunkumar V, Vasudevan M, Maduraimuthu V, and Muthupandi V, *Mater Manuf Proces* **27** (2012) 1171.
3. Dey H C, Albert S K, Bhaduri A K, Roy G G, Balakrishnan R, and Panneerselvi S, *Weld World* **58** (2014) 389.
4. Lee J S, and Maruyama K, *Metals Mater Int* **21** (2015) 639.
5. Mayr P, and Horst C, *Trans Indian Inst Metals* **63** (2010) 131.
6. Vuherer T, Marko D, LjMilovic M, and Ivan S, *Metalurgija* **52** (2013) 317.
7. Kalvala, P R, Akram J, Misra M, Ramachandran D, and Gabbita J R, *Defence Technol* **12** (2016) 285.
8. Kumar S S, Murugan N, and Ramachandran K K, *Int J Refract Metals Hard Mater* **58** (2016) 196.
9. Shen Y, Zhiqiang X, Kai C, and Jie Y, *J Nucl Mater* **455** (2014) 234.
10. Manugula V L, Koteswararao V R, Madhusudhan Reddy G, Mythili R, and Bhanu S R K, *Metallurg Mater Trans A* **48** (2017) 3702.
11. Husain, Md M, Sarkar R, Pal T K, Prabhu N, and Ghosh M, *J Mater Eng Perform* **24** (2015) 3673.
12. Ramesh R, Dinaharan I, Kumar R, and Akinlabi E T, *Mater Sci Eng A* **687** (2017) 39.